Boronate Ligands in Materials: Determining Their Local Environment by Using a Combination of IR/Solid-State NMR Spectroscopies and DFT Calculations

Saad Sene,[a] Marc Reinholdt,[a] Guillaume Renaudin,[b] Dorothée Berthomieu,[a] Claudio M. Zicovich-Wilson,[c] Christel Gervais,[d] Philippe Gaveau,[a] Christian Bonhomme,[d] Yaroslav Filinchuk,[e] Mark E. Smith,[f] Jean-Marie Nedelec,[b] Sylvie Bégu,[a] P. Hubert Mutin,[a] and Danielle Laurencin*[a]

Abstract: Boronic acids (R-B(OH)$_2$) are a family of molecules that have found a large number of applications in materials science. In contrast, boronate anions (R-B(OH)$_3^-$) have hardly been used so far for the preparation of novel materials. Here, a new crystalline phase involving a boronate ligand is described, Ca[C$_4$H$_9$-B(OH)$_3$]$_2$, which is then used as a basis for the establishment of the spectroscopic signatures of boronates in the solid state. The phase was characterized by IR and multinuclear solid-state NMR spectroscopy (¹H, ¹³C, ¹¹B and ⁴³Ca), and then modeled by periodic DFT calculations. Anharmonic OH vibration frequencies were calculated as well as NMR parameters (by using the Gauge Including Projector Augmented Wave—GIPAW—method). These data allow relationships between the geometry around the OH groups in boronates and the IR and ¹H NMR spectroscopic data to be established, which will be key to the future interpretation of the spectra of more complex organic–inorganic materials containing boronate building blocks.

Keywords: boron · density functional calculations · IR spectroscopy · NMR spectroscopy · solid-state structures

Introduction

Boronic acids (R-B(OH)$_2$) and boronates (R-B(OH)$_3^-$) have a wide range of applications in organic synthesis, in which they are notably used as reagents in Miyaura–Suzuki coupling reactions.[1] Boronic acids also play an important role in materials science,[1] for example, they are employed for the synthesis of covalent organic frameworks (COFs),[2] which can be used for gas storage, catalysis, or optoelectronics. In contrast, boronates have hardly been studied for materials chemistry applications. Indeed, it is only recently that they were proposed as building blocks for the preparation of hybrid organic–inorganic materials,[3] following an investigation of the structure of layered phenylboronate phases of

[a] S. Sene, M. Reinholdt, Dr. D. Berthomieu, Dr. P. Gaveau, Dr. S. Bégu, Dr. P. H. Mutin, Dr. D. Laurencin
Institut Charles Gerhardt de Montpellier, UMR 5253
Université de Montpellier 2, CC 1701
Place E. Bataillon, F-34095 Montpellier cedex 05 (France)
Fax: (+33) 4-6714-3852
E-mail: dlaurenc@univ-montp2.fr

[b] Dr. G. Renaudin, Prof. J.-M. Nedelec
Clermont Université, ENSCCF
Institut de Chimie de Clermont-Ferrand
BP 10448, F-63000 Clermont-Ferrand (France)
and
CNRS, UMR 6296, ICCF, F-63171 Aubière (France)

[c] Prof. C. M. Zicovich-Wilson
Facultad de Ciencias
Universidad Autónoma del Estado de Morelos
Av. Universidad 1001
Col. Chamilpa, 62209 Cuernavaca, Morelos (Mexico)

[d] Prof. C. Gervais, Prof. C. Bonhomme
LCMCP, UMR CNRS 7574, UPMC Université Paris 06
Collège de France, 11 place Marcelin Berthelot
75231 Paris Cedex 05 (France)

[e] Dr. Y. Filinchuk
Swiss-Norwegian Beamlines at ESRF, 6 rue Jules Horowitz
BP 220, F-38043 Grenoble (France)
and
Institute of Condensed Matter and Nanosciences
Université Catholique de Louvain
Place L. Pasteur 1, B-1348, Louvain la Neuve (Belgium)

[f] Prof. M. E. Smith
Vice-Chancellor's Office, University House
Lancaster University, Lancaster, LA1 4YW (UK)
and
Magnetic Resonance Centre, Department of Physics
University of Warwick, Coventry, CV4 7HS (UK)

📖 Supporting information for this article is available on the WWW under http://dx.doi.org/10.1002/chem.201203560.

general formula $M[C_6H_5\text{-}B(OH)_3]_2 \cdot x H_2O$ (M = Ca, Sr, Ba; x = 0 or 1).[3] In this work, phenylboronate anions (C_6H_5-$B(OH)_3^-$) were found to act as multidentate bridging ligands between alkaline-earth metal cations, making them interesting building units for the preparation of hybrid materials.

Although the study of alkaline-earth phenylboronates marked the first step towards the understanding of the coordination chemistry of boronate ligands, this field is still largely unexplored. In particular, their spectroscopic signatures in the solid state still need to be analyzed in detail, so that the local environment of boronates within more complex organic–inorganic materials can then be understood more easily. For instance, given that solid-state NMR is one of the main techniques available to characterize hybrid organic–inorganic materials, it is important to be able to relate the NMR spectroscopic data to local structural features around the ligand. The advantage of boronate ligands is that they contain several nuclei of interest for solid-state NMR spectroscopy, namely, ^1H, ^{11}B, and ^{13}C, for which high-resolution experiments can be carried out at natural abundance, and which may each provide complementary information on the local environment of boronates. IR spectroscopy is another technique which should be explored, as the vibration frequencies of the boronate OH groups are likely to inform on the hydrogen-bond (H bond) network around the boronate in the material. However, in the initial work on phenylboronates,[3] no precise link between the OH stretching frequency and the local geometry around the OH groups was proposed.

For an increasing number of complex materials, computational modeling is performed to assist in understanding their structure,[4] formation,[5] reactivity,[6] and spectroscopic data.[7] In particular, it has been shown that NMR parameters in materials can be calculated accurately by using the DFT GIPAW approach (Gauge Including Projector Augmented Wave).[8,9] This means that if a model structure of the material studied is proposed, the NMR parameters for this structure can be calculated by using GIPAW, and then compared to the experimental NMR spectra. When a good agreement between the experimental spectra and calculated data is obtained, this can help validate the model, as NMR spectroscopy is very sensitive to the local structure around an atom. This approach is commonly referred to as "NMR crystallography".[8,10] Similarly, it has been demonstrated that IR vibration modes can be calculated accurately for a wide variety of materials, and that this can be used to help interpret complex IR spectra, as demonstrated for heterogeneous catalysts like MgO.[7a] For boronic acids, calculations of IR and NMR parameters have already been reported,[11] but these were mainly performed on isolated molecules or dimers. It is only recently that Bryce and co-workers reported calculations of NMR parameters for periodic crystals of boronic acids.[11e,f] Concerning boronates, the only computational studies of NMR parameters concern the phenylboronate phases mentioned above.[3,12] It was shown that in the case of $Ca[C_6H_5\text{-}B(OH)_3]_2$, different models that differed in the orientation of the OH groups can be discriminated by

comparing experimental and calculated NMR spectra,[3] making NMR very attractive for the study of these materials. In contrast, calculations of IR data from boronate structures have not yet been reported, despite the fact that this could provide complementary insight into the arrangement around the hydroxyl groups, given the high number of different OH stretching frequencies observed on the IR spectra of phenylboronates.[3]

The aim of this study is to improve methodologies to determine material structures involving boronate ligands, in which cohesion forces based on H-bonds and weak van der Waals interactions are present, and to help make the best use of both the IR and NMR spectroscopies for the characterization of these phases. To this end, we mainly focus here on a new crystalline phase that involves an alkylboronate chain, calcium butylboronate. First, the synthesis and crystallographic structure of this new material is described, and the coordination chemistry of the boronate analyzed. The structure is characterized by several techniques, including IR and multinuclear solid state NMR spectroscopy (^1H, ^{11}B, ^{13}C and also natural abundance ^{43}Ca NMR spectroscopy). The exact atomic positions in the structure are then determined by using an NMR crystallography approach. Finally, both the Ca-butylboronate and the previously published Ca-phenylboronate structure are the subject of periodic DFT calculations of the ^1H NMR parameters and IR OH stretching frequencies, leading to a precise mode of identification of the different geometries of OH groups and H bonds in boronates, based on ^1H NMR and IR spectra.

Results and Discussion

Synthesis of Ca-butylboronate and description of its crystal structure: Calcium butylboronate was synthesized by following the procedure previously established for $Ca[C_6H_5\text{-}B(OH)_3]_2$ (CaBPh),[3] by precipitating a solution of C_4H_9-$B(OH)_3^-$ by Ca^{2+}. The microcrystalline powder obtained corresponds to $Ca[C_4H_9\text{-}B(OH)_3]_2$ (CaBBu), according to elemental and thermogravimetric analyses (see the Experimental Section and Figure S1, Supporting Information).

Powder X-ray diffraction and electron microscopy confirm the crystallinity of the sample (Figure 1). On the powder pattern, the strongest peak at small angles corresponds to an interplanar distance of 16.4 Å, which suggests that the phase has adopted a lamellar structure, by analogy with previous work on phenylboronates and phenylphosphonates.[3,13] Rietveld refinements were carried out on the diffractogram recorded with synchrotron radiation, confirming the layered structure of the material (Figure 1B). CaBBu is composed of layers of Ca^{2+} interconnected through butylboronate ligands, with the alkyl chains facing each other in the interlayer space. The calcium is in an eight-coordination environment, and is bound to the OH groups of six different butylboronate ligands. There are two independent boronate ligands in the unit cell, which both play the role of bridging ligands between three Ca^{2+} cations (Figure S2, Supporting
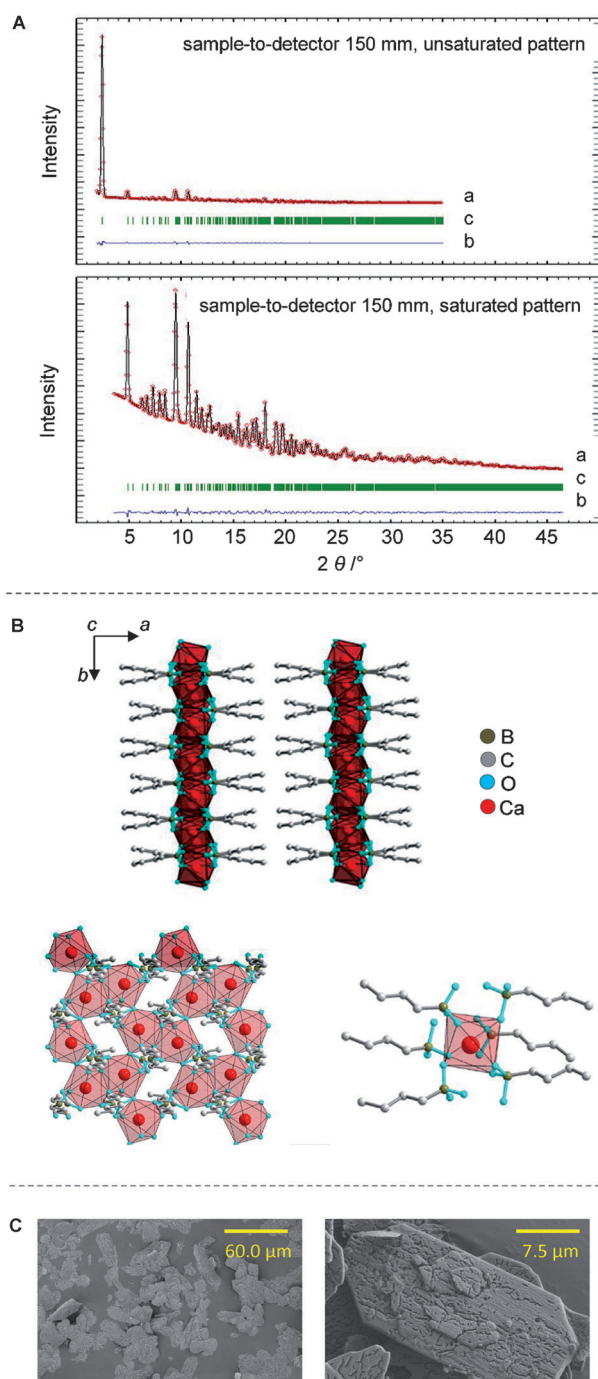
Figure 1. A) Rietveld plots of Ca-butylboronate for the two out of the four used patterns. Observed (red dots) and calculated (solid lines) synchrotron ($\lambda = 0.697751$ Å) powder diffraction patterns (a), difference curves (b) and Bragg peak positions (c). B) General representations showing the layered structure of Ca[C$_4$H$_9$-B(OH)$_3$]$_2$, the calcium arrangement in alkaline-earth slabs, and the polyhedron of eightfold coordinated calcium cations. C) SEM images of Ca[C$_4$H$_9$-B(OH)$_3$]$_2$.

Information). This actually marks a difference compared to the Ca-phenylboronate structure, in which the boronate ligands were only bridging two Ca^{2+} cations, leading to the formation of chains of Ca-phenylboronate, which then interacted through H bonds to form a layered structure.[3]

Solid-state NMR and IR spectra: The previous study of phenylboronate phases had shown that IR and multinuclear solid-state NMR can be used to shed light on the H-bond network in these materials, and thereby help understand more precisely their structure at the molecular level. The ^{11}B, ^{13}C, ^{1}H, and ^{43}Ca magic-angle spinning (MAS) NMR spectra of CaBBu are shown in Figure 2.

The ^{11}B MAS NMR lineshape suggests that the two independent boron sites have very similar NMR spectroscopic parameters. It should be noted that this phase was characterized several times by ^{11}B MAS NMR spectroscopy at different magnetic fields, because distortions in the lineshape were often observed on the low frequency side of the signal (Figure S3, Supporting Information), deviating from the expected superimposition of two "pure quadrupolar lineshapes". In a previous ^{11}B NMR spectroscopic study of aryl-
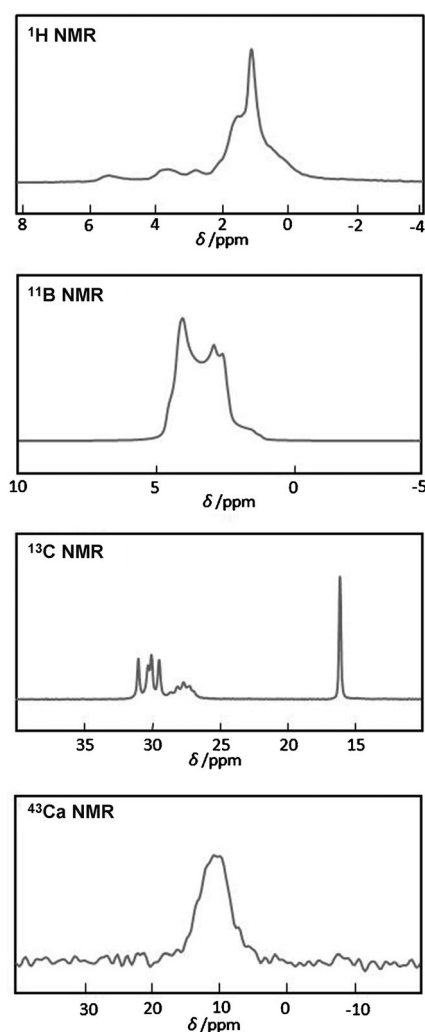

Figure 2. MAS NMR spectra of Ca[C$_4$H$_9$-B(OH)$_3$]$_2$: ^{1}H (14.1 T, 10 kHz MAS, DUMBO—see also Figure S9, Supporting Information), ^{11}B (14.1 T, 20 kHz MAS, single-pulse excitation with ^{1}H decoupling, sample physically diluted in SiO$_2$—see also Figure S3, Supporting Information), ^{13}C (14.1 T, 10 kHz MAS, CPMAS with ^{1}H decoupling, 2 ms CT), and ^{43}Ca NMR (14.1 T, 4 kHz MAS, single-pulse excitation with double frequency sweep (DFS)[17] enhancement).

boronic acids and their catechol cyclic esters, Bryce and co-workers had also reported lineshape distortions, which were found to be caused by the use of hard pulses and by anisotropic relaxation effects.[11e] Here, neither the pulse power nor the relaxation were found to affect the lineshape (Figure S4, Supporting Information). However, the preferential orientation of the crystallites within the rotor was found to have an influence (Figure S3, Supporting Information), and this problem can be partly circumvented by physically diluting the sample in silica. The two independent [11]B sites were then resolved by using a 3Q-MAS[14] experiment (Figure S5, Supporting Information), from which the NMR parameters of each site were extracted. These are consistent with the ones measured for Ca-phenylboronate (Ca[C_6H_5-B(OH)$_3$]$_2$, CaBPh), with only slightly higher C_Q and δ_{iso} values (Table S1, Supporting Information). The origin of this small difference in [11]B parameters is still under investigation at this stage.

The ^{1}H–^{13}C cross-polarization MAS (CPMAS) NMR spectrum of CaBBu recorded at room temperature shows the presence of five distinct peaks (at $\delta = 16.0$, 29.4, 29.9, 30.2, and 30.9 ppm) and one complex multiplet (centered at $\delta = 27.6$ ppm; Figure 2). Eight distinct signals were a priori expected, due to the nonequivalence of the butyl chains in the crystal structure. The signal at $\delta = 16.0$ ppm can be assigned to overlapping resonances from the two CH$_3$ carbon atoms. The signals from the middle carbon atoms of the butyl chains are all between $\delta = 29.4$ and 30.9 ppm, with, in this case, four distinct resonances, as expected from the crystal structure. ^{13}C{^{11}B} REDOR (rotational echo double resonance)[15] experiments were carried out to further assign each of these resonances, as the dephasing observed of the ^{13}C signals depends on the C···B distances (Figure S6, Supporting Information). As shown in the REDOR spectrum, Figure 3, the two highest frequency signals correspond to the CH$_2$ groups closest to the B. The multiplet at $\delta = $ ~27.6 ppm is due to the two C atoms attached to the B; the complex form of the peak is due to J couplings with neighboring ^{11}B and ^{10}B isotopes, as well as residual dipolar/quadrupolar interactions.[11e] It is noteworthy that all ^{13}C resonan-

ces are particularly sharp, leading to a very well-resolved spectrum in comparison with the data recorded so far on phenylboronate structures, and that the relative positions of the different ^{13}C resonances observed here for CaBBu are in agreement with ^{13}C solution NMR spectra of butylboronate anions in water (Figure S7, Supporting Information).

Natural-abundance ^{43}Ca MAS NMR spectra were also recorded at two different magnetic fields,[16] because the study on Ca-phenylboronate had shown that ^{43}Ca NMR spectroscopy can be useful to discriminate between different models of the structure.[3] For CaBBu, only one featureless lineshape was observed, which was simulated by fitting the data recorded at the two fields (Figure S8, Supporting Information), considering the presence of only one Ca site (as in the experimental crystal structure). The ^{43}Ca parameters measured ($\delta_{iso} = 14.6 \pm 2.0$ ppm, $C_Q = 1.50 \pm 0.15$ MHz, $\eta_Q = 0.60 \pm 0.15$) were consistent with those found so far for Ca–organic complexes,[16c] including Ca-phenylboronate.[3]

The ^{1}H NMR spectrum of CaBBu was recorded at 600 MHz by using the w-DUMBO[18] sequence (Figure 2 and Figure S9, Supporting Information). It shows the presence of an intense signal centered at $\delta = $ ~1 ppm, corresponding mainly to protons from the alkyl chain. Other shoulders at higher chemical shifts are also present on the spectrum (notably at $\delta > 5$ ppm), which are likely to correspond to OH groups involved in H bonds. IR spectroscopy confirms the presence of fairly strong H bonds, with a broad OH stretching band centered at $\sigma = $ ~3326 cm^{-1} (Figure 4 and Figure S10, Supporting Information). This band is actually at lower wavenumbers compared to the broad OH bands previously observed for CaBPh, which suggests that the H bond is actually stronger in the CaBBu phase. Other OH groups not involved in H bonds are also present in the structure, as attested by the sharp OH stretching band; their ^{1}H chemical shift actually overlaps with those of the butyl chain protons.

Modeling of the Ca-butylboronate structure and calculation of NMR spectroscopic parameters: To determine the position of the H atoms in the structure,[19] and also to locate
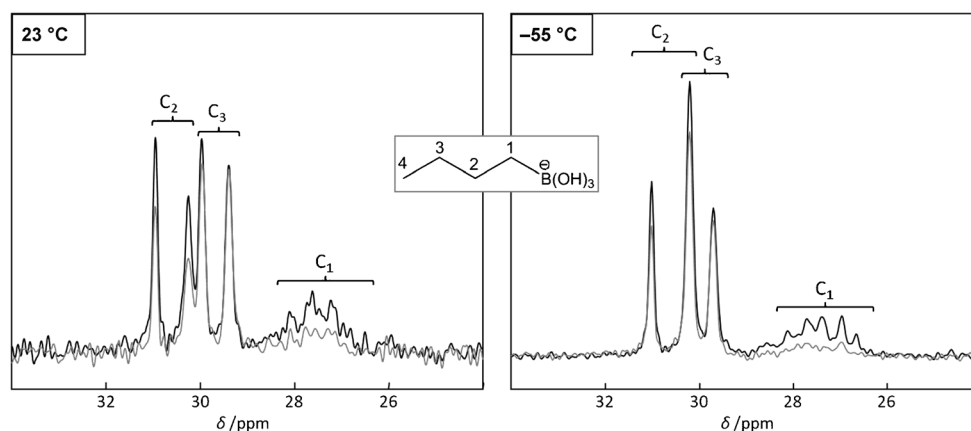

Figure 3. ^{13}C{^{11}B} REDOR NMR spectra of Ca[C_4H_9-B(OH)$_3$]$_2$, recorded at 23 and −55 °C. Spectra acquired by using a total dephasing time of 4.8 ms, with (gray line) or without (black line) π pulses on the ^{11}B spectrum.
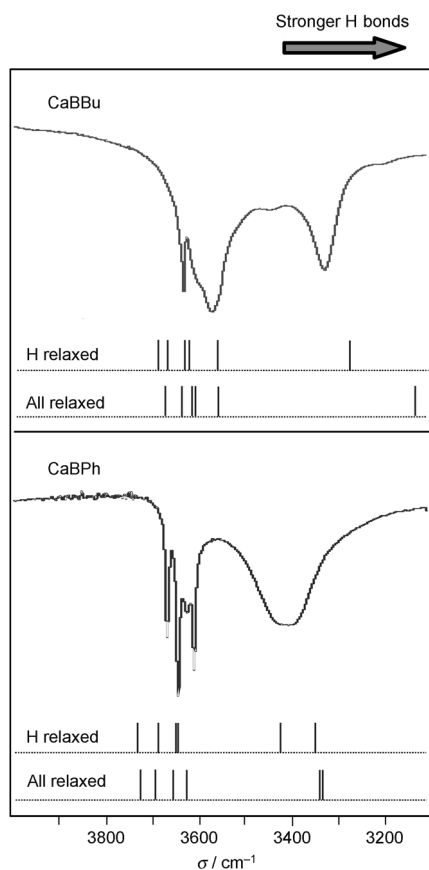
Figure 4. Experimental and calculated OH stretching vibrations of Ca-[C$_4$H$_9$-B(OH)$_3$]$_2$ (CaBBu) and Ca[C$_6$H$_5$-B(OH)$_3$]$_2$ (CaBPh). Anharmonic OH frequencies calculated for H-relaxed and fully relaxed models are shown as vertical bars.

ally. Each relaxed structure was analyzed in detail. It turned out that in some cases, the calculations converged towards a local energy minimum, with unexpected and unlikely structural features, such as very short Ca···H distances (~2.28 Å). Of all the configurations tested, the most stable one had only one O–H···O hydrogen bond.[22]

For the most stable H-relaxed model, the ^{1}H, ^{13}C, ^{11}B, and ^{43}Ca NMR spectroscopic parameters were calculated by using the GIPAW approach, and the corresponding NMR spectra were simulated. The comparison between experimental and calculated spectra is shown in Figure 5. Clearly, discrepancies can be noticed, mainly in the calculated ^{13}C NMR spectroscopic resonances.[23] Indeed, the calculated ^{13}C chemical shifts for the "C$_3$" carbon atoms (3rd down the butyl chain, when starting from the B) are at $\delta = ~36$ ppm, which is much higher than the experimental values ($\delta = 29.4$ and 29.9 ppm), and actually leads to an inversion of the positions of the C$_2$ and C$_3$ atoms in the calculated spectrum.

The model resulting from the relaxation of H positions only being unsatisfactory, additional calculations were carried out, in which C, B, O, and Ca atoms of the CaBBu structure were successively relaxed, revealing that relaxations of C, O, and B positions are energetically most relevant (Table 1). Slight modifications in bond lengths were observed upon these relaxations (Table S2, Supporting Information), but the number of H bonds remained unaffected. For each model, NMR spectroscopic parameters were calculated (Figure 5 and Tables S3–S5, Supporting Information). The additional relaxations do not significantly affect the calculated ^{1}H, ^{11}B, and ^{43}Ca NMR spectroscopic data, as the spectral simulations produce similar results as in the H-relaxed model. In contrast, when comparing the calculated ^{13}C NMR spectroscopic data with the experimental one, it appears that additional C relaxation helps to improve the
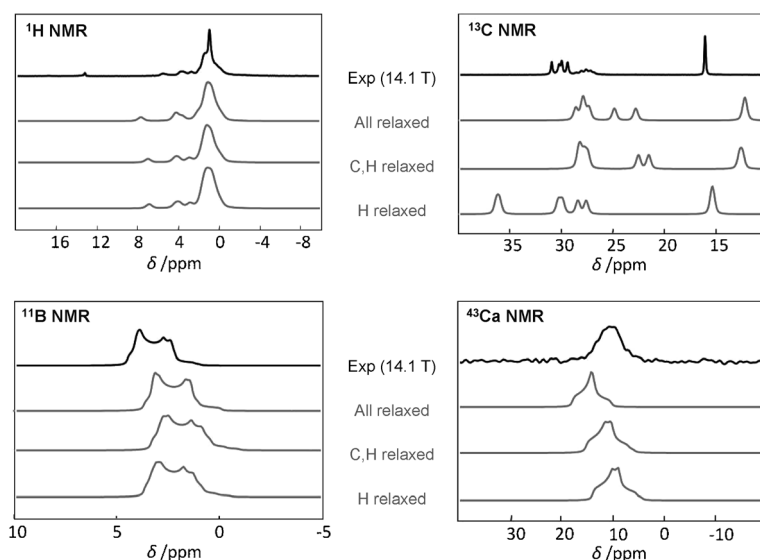
more precisely the other elements, periodic LCAO-B3LYP D* calculations were considered,[20] which include the Grimme correction to take into account the weak dispersion forces. When looking closely at the O···O bond lengths in the experimental crystal structure, it seems clear that there are several short O···O distances (<2.9 Å), which could allow "moderate"[21] H bonds between different butylboronate ligands to be established. With this in mind, different possible orientations for the OH groups within the crystal lattice were proposed, by starting from the experimental XRD crystal structure (Exp-R1). For each configuration, the H positions were then relaxed computation-

Figure 5. Experimental ^{1}H, ^{11}B, ^{13}C, and ^{43}Ca MAS NMR spectra of Ca[C$_4$H$_9$-B(OH)$_3$]$_2$ (black lines), and spectra simulated after GIPAW calculations for different models of the structure (gray lines). Details on the parameters used for the MAS spectra can be found in the Experimental Section.

Table 1. Structural models on which geometry optimizations and calculations of IR vibrational modes or NMR spectroscopic parameters were carried out.

	Optimized atomic positions	Grimme correction	Final energy per unit cell [Hartree]	Grimme correction per unit cell [Hartree]	IR calculations	GIPAW NMR calculation
Ca-butylboronate	H	yes	−5992.8415	−0.4016	yes	yes
	C,H	yes	−5992.9857	−0.4044	no	yes
	C,H	no	−5992.6661		no	yes
	C,H,O,B	yes	−5993.0774	−0.4067	no	yes
	C,H,O,B,Ca	yes	−5993.1030	−0.4086	yes	yes
Ca-phenylboronate	H	yes	−3291.6475	−19.6348	yes	yes
	C,H,O,B,Ca	yes	−3291.6723	−19.7560	yes	yes

ture, the system becomes more rigid, leading to changes in the C_2 and C_3 isotropic chemical shifts.

Although low-temperature experiments help rationalize the relative order of the different ^{13}C resonances, discrepancies remain between the spectra calculated from the experimental models and those recorded experimentally. In particular, concerning the ^{13}C NMR spectroscopic data, all resonances
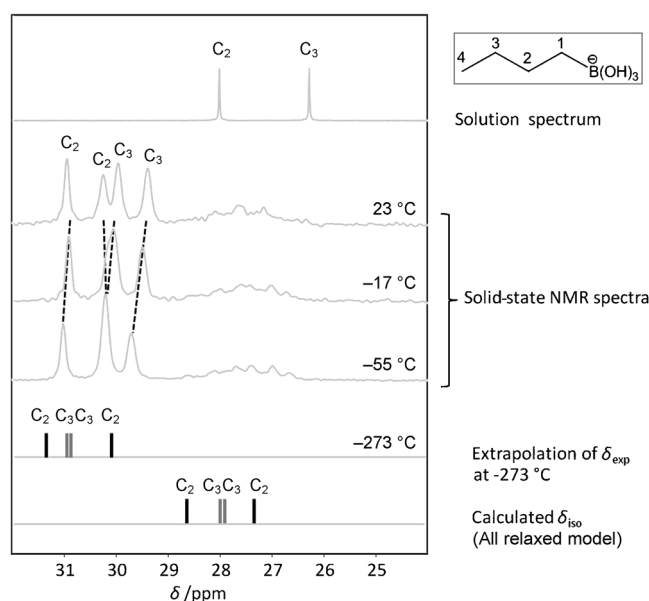
modeling of the butyl chain, because ^{13}C resonances of the C_2 and C_3 atoms become much closer in chemical shift (Table S4, Supporting Information). This can be explained by the changes in the C_2–C_3 and C_3–C_4 bond lengths which occur upon relaxation of the C positions (Table S2, Supporting Information). However, even when all atoms in the structure are relaxed, discrepancies remain for the C_1 and C_4 chemical shifts, and the highest frequency signal still belongs to a C_3 atom, in disagreement with the REDOR assignment reported above.

In previous studies aimed at comparing experimental and calculated NMR chemical shifts in organic and inorganic compounds, it has been shown that better agreement between calculated and experimental chemical shifts can be reached by taking into account temperature effects.[24] Indeed, while GIPAW calculations are performed at ~0 K, NMR spectroscopic experiments are often performed at room temperature, and this can be at the origin of discrepancies between the two. Thus, to see if a better agreement between experimental and calculated NMR spectroscopic parameters could be observed for the Ca-butylboronate structure, additional ^1H-^{13}C CPMAS NMR spectra were thus recorded at decreasing temperatures down to −55 °C (Figure 6), and $^{13}C\{^{11}B\}$ REDOR experiments were performed to assist in the assignment of C_2 and C_3 resonances at each temperature (Figure 3). Clearly, when performing experiments at lower temperatures, changes in the isotropic chemical shifts of C atoms are observed, with the C_3 resonances being the most affected. The expected experimental chemical shifts at 0 K were thus extrapolated by linear regression (Figure S11, Supporting Information), which shows that the relative order between C_2 and C_3 resonances becomes consistent with GIPAW calculations (Figure 6). It should be noted that ^1H DUMBO NMR spectra were also recorded at low temperatures (down to −50 °C), but that no changes in peak positions were observed, in contrast with ^{13}C NMR spectra. The variations in ^{13}C chemical shifts with temperature may be caused by changes in "mobility" of the butyl chain in CaBBu, which may be reflected in C_2 and C_3 chemical shifts mainly: at room temperature, the C_2 and C_3 resonances have the same relative positions as in ^{13}C solution NMR spectra, whereas when decreasing the tempera-

Figure 6. Temperature-dependance of the δ_{iso} position of the C_2 and C_3 atoms of the butyl chains of Ca[C_4H_9-B(OH)$_3$]$_2$, and comparison with the calculated ^{13}C NMR spectroscopic chemical shifts. Details on the parameters used for recording the CPMAS spectra can be found in the Experimental Section.

calculated by GIPAW for the fully relaxed structure are ~2 to 5 ppm below the experimental ones, being most noticeable for C_1 and C_4 resonances, even after extrapolation at 0 K. A systematic shift in calculated ^{13}C resonances had also been observed for Ca-phenylboronate, but towards higher frequencies.[3] An explanation of this discrepancy may be that some of the empirical parameters in the Grimme correction need to be adjusted,[25] or that there are some basis set or DFT functional choice effects in the calculations. We did not attempt to test these points, as it was beyond the scope of this work.

Overall, from this modeling study of Ca-butylboronate, it is clear that starting from the experimental atomic positions of the Exp-R1 refined structure, once all protons have been positioned, the relaxation of the H atoms only does not provide a reasonable model of the structure. Further relaxations

of the other atomic positions (mainly C) are thus necessary, in line with the previous study of Ca-phenylboronate.[3] Based on the fully relaxed model of Ca-butylboronate, more accurate values of interatomic bond lengths (especially C−C lengths) were derived, and the experimental XRD data were thus re-refined with more restrictive constraints (Exp-R2 structure), to offer a more accurate description of the CaBBu structure.

IR vibration frequencies and ^{1}H chemical shifts of the OH groups: The representations of the local environment of the hydroxyls in the fully relaxed models of CaBBu and CaBPh are shown in Figure 7. Simple geometrical considerations allow the OH groups to be classified into three categories: 1) those involved in a fairly strong H bond (d(OH···O) < 1.9 Å),[26] 2) those for which the closest O atom neighbor is more than 2.8 Å distant ("free" OH groups), and 3) those that are between these two situations (for which the shortest OH···O distance is between 2.1 and 2.4 Å).

More detailed analyses of the geometry of the H bonds can be used to account for the differences in IR and NMR spectroscopic data between CaBBu and CaBPh. This is particularly true when looking at the strongest H bonds in these structures. Indeed, for CaBBu, the strongest H bond is characterized by an OH···O distance of 1.728 Å and an O-H-O angle of 172.6°, which means that it is stronger and more directional than the two strongest H bonds in CaBPh (OH···O distances of 1.834 and 1.843 Å and O-H-O angles of 159.1 and 165.5°). This explains the differences in O−H stretching frequencies between CaBPh and CaBBu below 3500 cm^{-1} (Figure 4).

When considering both Ca-butylboronate and Ca-phenylboronate phases, it is clear that all the other OH groups
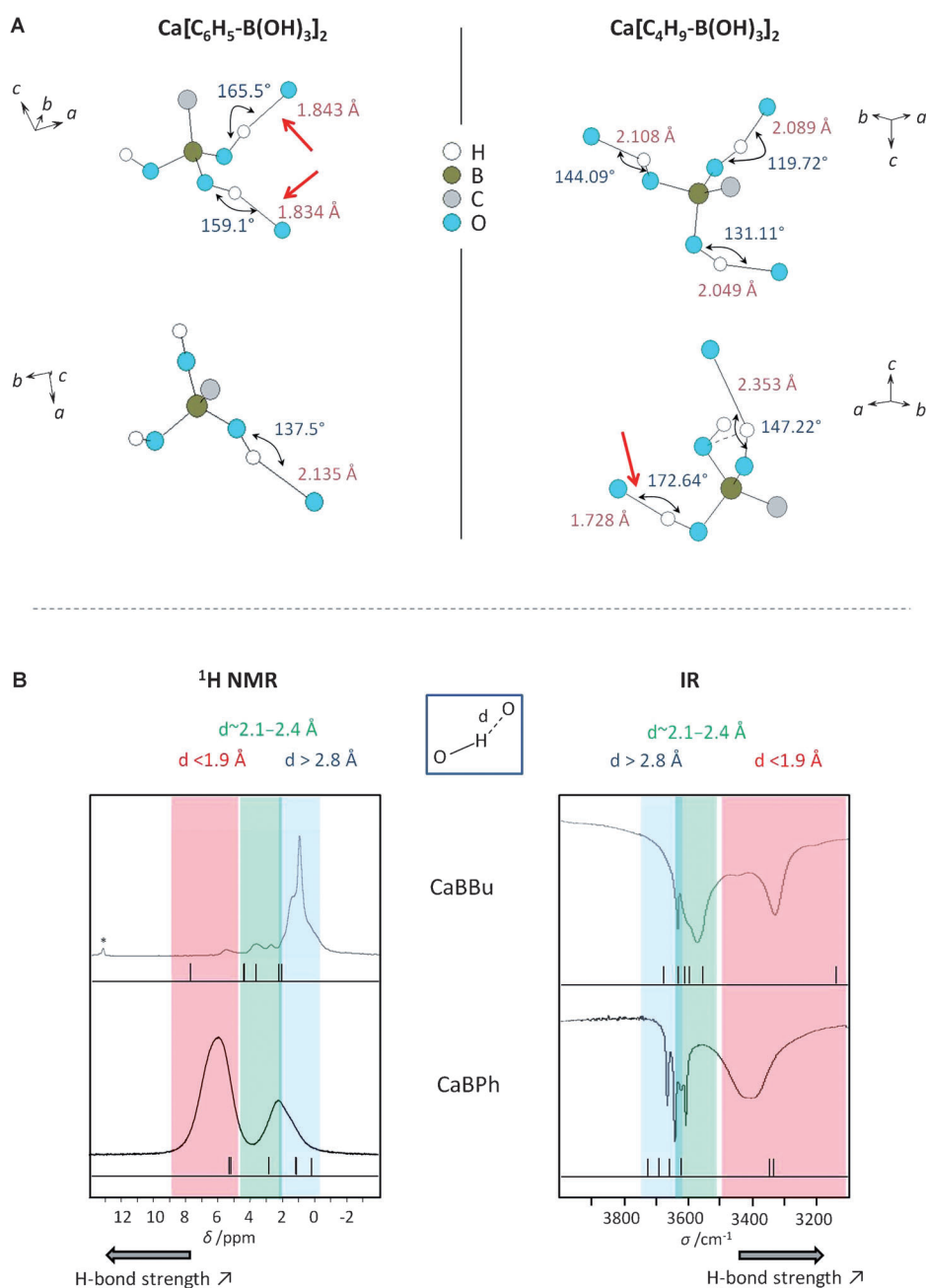

Figure 7. A) Representation of the local geometries around the OH groups in the all-relaxed models of Ca-[C$_4$H$_9$-B(OH)$_3$]$_2$ (CaBBu) and Ca[C$_6$H$_5$-B(OH)$_3$]$_2$ (CaBPh). For each structure, the two symmetrically independent boronate ligands are shown, but the organic chain is not represented for clarity. The strongest H bonds are pointed out by using red arrows. B) Relationships between O−H stretching frequencies and ^{1}H chemical shifts, and the OH···O distance in the H bonds. The calculated ^{1}H chemical shifts of the OH groups and OH anharmonic stretching frequencies for the fully relaxed CaBBu and CaBPh are shown as vertical bars below the experimental spectra (see also Table S6, Supporting Information). Contributions of the ^{1}H resonances of the organic chains are not discussed in the figure.

cover a wide range of ^{1}H chemical shifts and IR stretching frequencies, and it is naturally appealing to try to relate these chemical shifts and vibration frequencies to the local structures around the OH. Thus, in addition to the GIPAW calculations of ^{1}H chemical shifts, the anharmonic vibration frequencies of the OH groups were calculated for different

structural models of these two phases (Table S6, Supporting Information).

The comparison between calculated and experimental vibration frequencies is shown in Figure 4. Globally, calculations reproduce well the separation between the strongest H bonds (< 3500 cm^{-1}) and all the others (> 3500 cm^{-1}). However, a rather large discrepancy in the calculated wavenumber for the strongest H bonds is noticeable for the fully relaxed models of both CaBPh and CaBBu (> 100 cm^{-1} for CaBBu). This is probably due to the fact that the anharmonic frequencies are computed by sampling points along the O−H bond direction, assuming this is the actual mode direction, which may not be true when the H atom is affected by H bonds with neighboring oxygen atoms. Concerning all the OH groups with vibration frequencies > 3500 cm^{-1}, smaller discrepancies between calculated and experimental values are observed for the fully relaxed models of CaBBu and CaBPh relative to the H-relaxed models (Figure 4 and Table S6, Supporting Information). This is consistent with the fact that the fully relaxed structures correspond to a more accurate description of the structure of these phases, as shown by the NMR crystallography study (see above and ref. [3]).

Based on the calculated IR and NMR parameters, it is now possible to relate different ranges of IR wavenumbers and ^{1}H chemical shifts to a given OH···O distance (Figure 7B). This clearly shows that the three categories of OH groups described above lead to three distinct regions on the IR and ^{1}H NMR spectra, with little overlap between the different regions. It should be noted that the OH···O distance is the only geometrical parameter that allowed such trends to be defined for the two boronate structures, which is not fully surprising given that in several other studies aimed at relating H-bond structures to ^{1}H chemical shifts in materials, this is also the geometrical parameter which has been used.[27] The information summarized in Figure 7B demonstrates the complementarities of IR and NMR spectroscopies for establishing local environments of boronates in materials, and the added value of recording IR spectra of these phases. Indeed, the OH stretching frequencies do not overlap with other vibration modes on the IR spectra and may thus provide direct insight on structural features around the hydroxyls. In contrast, ^{1}H chemical shifts of the OH groups can overlap with signals from the organic chain and may thus be "masked" in a simple 1D spectrum. Such information is priceless for the understanding of the structure of future boronate-containing materials for which a crystal structure would not be available, as it will help to shed light on the way in which the boronate ligand can be involved in H bonds within the material, and help propose more accurate models of the material.

Interactions within the Ca-butylboronate and Ca-phenylboronate structures: With the prospect of using boronate ligands for developing new materials, we decided to look in more detail into the different possible molecular interactions leading to the CaBBu and CaBPh crystal phases. Indeed, although both structures have an overall layered organization, discrepancies can be noticed.

The cohesion within the CaBBu and CaBPh planes of cations is ensured by the boronate ligands which 1) bridge different Ca^{2+} cations and 2) establish H bonds between each other. Differences in the modes of interaction between these boronate ligands are observed in the structures, both in the number of H bonds they are involved in and in the number of metal cations to which they bind, as summarized in Figure S12, Supporting Information.

The interactions between the organic chains are weaker, as they involve dispersion forces. Given that the Grimme correction includes the van der Waals interactions, the global contribution of van der Waals interactions to the overall stability of the unit cell was calculated. As shown in Table 1, the Grimme correction represents only ~0.60 and 0.0067% of the total energy of the fully-relaxed structures of the CaBPh and CaBBu phases, respectively. The much lower contribution of the Grimme correction in the case of the CaBBu structure can be explained by the overall lower density of this phase, relative to CaBPh. Indeed, given that the van der Waals interactions vary as $1/r^6$, they will be much weaker if the structure is less dense, that is, if the atoms are in average more separated. As a direct consequence of the lower density of the CaBBu structure, the interactions between chains of neighboring boronate ligands in CaBBu will be weaker than in the CaBPh system. This may be one of the reasons for the presence of defects and "holes" at the surface of the crystallites of CaBBu (Figure 1C), such defects not having been observed previously in the case of CaBPh. Indeed, having carefully analyzed the different experimental parameters which may have caused the formation of these defects (see the Supporting Information for details, Figures S13–S15), it appears that these are mainly due to the nature of the organic chain bound to the boron. The formation of surface defects in the case of CaBBu would result of an imperfect growth of the crystals during the precipitation of the material, the driving force for completely filling some of the layers with butylboronates being too weak, due to the weak interactions between neighboring butyl chains. In contrast, for CaBPh structures, the stronger interactions between neighboring phenylboronates[3] leads to a complete filling of each layer, thereby preventing the formation of such defects.

In the previous study of Ca-phenylboronate phases, we had shown that the material does not appear to have the propensity to exfoliate and allow the intercalation of other organic molecules between the layers. Here, in a similar fashion, we were unable to intercalate organic molecules in the interlayer space of the CaBBu structure. Indeed, attempts to intercalate molecules like pyrene or 1,8-diaminonaphtalene between the butyl chains were unsuccessful, whatever the synthetic strategy attempted. Such behavior may appear as strange for the butyl system, given the low density of packing and the overall weakness of the van der Waals interactions. Thus, a possible explanation for the absence of intercalation properties of CaBBu is that it would

require exposing some of the butyl chains to the solvent and cause a disruption in the order between the chains in the layers, both situations being energetically unfavorable and creating disorder in the system.

Overall, this comparative analysis of CaBPh and CaBBu structures points to structural and textural modifications that can be observed in boronate materials, when varying the nature of the organic chain bound to the boron. Such considerations may help guide the choice of which type of boronate ligand to choose in future syntheses of more complex boronate-containing materials.

Conclusion

By studying $Ca[C_4H_9\text{-}B(OH)_3]_2$, progress has been made in the understanding of the coordination chemistry of boronate ligands and in the determination of their spectroscopic signatures in the solid state. On one hand, new possible bridging modes have been found for boronate ligands, which complement those previously observed for phenylboronate structures. On the other hand, by performing DFT calculations of NMR spectroscopic parameters and anharmonic OH stretching frequencies, it was possible to relate parts of the experimental IR and ^1H NMR spectra to signatures of hydroxyl groups, involved in H bonds of varying strengths, as quantified here by changes in OH···O distances. Both points mentioned above are particularly valuable in determining how boronates can be used as building blocks for the preparation of more complex hybrid organic–inorganic materials, and to be able to establish their local environment with precision within these solid phases. More generally, similar strategies, which combine both experiments and computations, would deserve to be applied more often for the design and study of new families of ligands.

As a result of the work we carried out here on Ca-butylboronate, and the comparison we made with our previous work on phenylboronates, the following experimental/computational methodology can now be proposed for future investigations of the structure of boronate containing materials, whether crystalline or disordered. First, high-resolution solid-state NMR spectra should be recorded on the material, making sure that several different nuclei are analyzed (^1H, ^{13}C, ^{11}B, and even metal cations like ^{43}Ca). Spectral editing should be performed by using dedicated pulse sequences, and NMR parameters extracted for each nucleus, taking into account possible variations in these parameters with temperature. In parallel, IR spectra should be recorded to determine the different kinds of OH groups in boronates, the possible presence of H bonds, and the range of variation of OH···O distances (by using the information summarized in Figure 7B). From the NMR and IR spectra recorded, detailed information on the local structure around the boronate will have been obtained, which can then be used to elaborate a sophisticated structural model of the material. Once fully relaxed employing a hybrid-DFT approach (including the weak van der Waals interactions in the theoreti-

cal description), the validity of this model can be tested, by checking whether the NMR and IR spectroscopic parameters are consistent or not with those observed experimentally. This robust strategy is currently being applied in our group to the analysis of other organic–inorganic materials involving boronates.

Experimental Section

Synthesis of $Ca[C_4H_9\text{-}B(OH)_3]_2$ (Ca-butylboronate, CaBBu): For the synthesis of CaBBu, butylboronic acid ($C_4H_9\text{-}B(OH)_2$, Alfa Aesar, 98+%), calcium chloride dihydrate ($CaCl_2\cdot2H_2O$, 99+% purity, Acros Organics), and sodium hydroxide (NaOH, Acros Organics) were used as received, and reactions were carried out by using ultrapure water and absolute ethanol.

The synthesis of CaBBu was performed as follows. Microbeads of NaOH (192.4 mg, 4.81 mmol) were dissolved in a (1:1) H_2O/EtOH mixture (14 mL). Butylboronic acid (489.7 mg, 4.8 mmol) was then added to the solution under magnetic stirring. After dissolution of the boronic acid, an aqueous solution of $CaCl_2\cdot2H_2O$ at 118.018 g L^{-1} (2.4 mmol, 3 mL) was added dropwise, leading to the immediate formation of a white precipitate. The suspension was stirred for ~30 min at room temperature.[28] The suspension was then filtered on a sintered glass frit under vacuum, maintaining the vacuum for 15 min. The precipitate was then washed twice with a (1:1) H_2O/EtOH mixture (10 mL), the vacuum being maintained for 15 min after each wash, and then twice with diethylether (10 mL), the vacuum being maintained for 5 min after each wash. The white powder was then dried in a furnace at 40°C for ~3 days. Yield: 570 mg (85%); elemental analysis calcd (%) for $C_8H_{24}B_2O_6Ca$: C 34.6, H 8.6, Ca 14.4, B 7.8; found: C 33.7, H 8.7, Ca 14.6, B 7.4. Attempts to recrystallize this sample to obtain single crystals were unsuccessful.

Characterization of $Ca[C_4H_9\text{-}B(OH)_3]_2$: Elemental analyses were carried out by the Service Central d'Analyse of the CNRS (Vernaison, France). IR spectra were recorded in transmission mode on KBr pellets, by using an Avatar 320 FTIR spectrometer.

SEM measurements were conducted on a Hitachi S4800 instrument under an excitation voltage value between 2 and 8 kV depending on the powder's surface charging. Powdered samples were deposited on double-face tape and then Pt-metallized by sputtering under vacuum.

Synchrotron powder X-ray diffraction measurements, indexation, and structure analysis: Since no crystals suitable for single-crystal X-ray diffraction were obtained, high-resolution X-ray diffraction powder patterns were recorded. Synchrotron powder diffraction data were obtained at Swiss-Norwegian Beam Lines at ESRF (Grenoble, France). The sample was introduced into 0.5 mm diameter glass capillaries. Data collections were performed at 295 K with a MAR345 Image Plate detector by using a monochromatic wavelength of $\lambda = 0.697751$ Å. The calculated absorption coefficient $m\mu R$ (m = powder packing factor, μ = linear absorption coefficient, R = radius of the capillary) was estimated as 0.12. Two sample-to-detector distances were used (150 and 400 mm) to combine the advantages of high structural and angular resolutions. Due to the very high relative intensity of the first diffraction ring, two exposure times were used for each sample-to-detector distance: one measurement with a non-saturated first ring (to have the exact relative intensities for all the diffraction peaks) and one measurement with a saturated first ring to increase the statistic counting for the low relative intensity diffraction peaks. The detector parameters and the wavelength were calibrated with NIST LaB$_6$. The highest resolution of the MAR345 detector was used: 3450×3450 pixels with a pixel size of 100 μm. During the exposure time the capillaries were rotated by 60°. The 2D data were integrated with Fit2D program.[29] Highly accurate integrated intensities were obtained thanks to a good powder average achieved by projecting the whole scattering information on the 2D detector. Uncertainties of the integrated intensities were calculated at each 2θ-point by applying Poisson statistics to the intensity data, and considering the geometry of the detector.[30]

The first 20 observed reflections from the nonsaturated data with the large sample-to-detector distance (high angular resolution) were used for indexing the unknown patterns. The DICVOL04 indexing program[31] was successfully used to reveal the monoclinic lattice of Ca-butylboronate, and systematic extinctions indicated space group $P2_1/c$. A Le-Bail fitting was performed by using the FULLPROF.2k program.[32] The peak shape was described with a Thomson–Cox–Hasting function. The profile matching refinements by using the nonsaturated measurements recorded with a sample-to-detector distance of 400 mm agree with the monoclinic $P2_1/c$ space group: $R_p = 4.57\%$ and $R_{wp} = 5.79\%$ with $a = 16.4304$ (6), $b = 8.3971$ (2), $c = 9.8668$ (4) Å and $\beta = 90.480$ (3)° ($V = 1361.25$ (1) Å³).

The structure was then solved in the centrosymmetric group $P2_1/c$ by the global optimization of the structural model in direct space by using simulated annealing (in parallel mode) with the FOX program.[33] As a cost function, the integrated wR factor of the unsaturated short sample-to-detector distance pattern[34] and anti-bump function (based on the minimal lengths Ca–O: 2.3, Ca–B: 2.5, Ca–C: 2.5, and Ca–C 3.5 Å) weighted at 0.60/0.40 were used. One independent $Ca(C_4BO_3)_2$ object was considered (corresponding to 4 motifs per unit cell in agreement with the expected density of the compound). The introduced $Ca(C_4BO_3)_2$ object was described as follows by 17 atoms (1 Ca, 2 B, 6 O, and 8 C): with bond lengths Ca–O: 2.40, B–O: 1.50, B–C: 1.60, and C–C: 1.55 Å, and angles O-B-O 109.5, O-B-C 109.5, B-C-C 115, and C-C-C 109°. The Ca-O-B angles were not restrained to solve the orientation of the organic chain around the alkaline-earth cation. H atoms were not considered here due to their weak scattering contrast for X-rays. The position of the central Ca atoms was allowed to vary, as well as the two Ca-O-B angles, with the use of the Dynamical Occupancy Correction for the automatic identification of the special crystallographic positions. The solution, with the x coordinate of Ca close to 0, was slowly found with all atoms in the general $4e$ position.

The crystal structure was refined by the joint Rietveld method by using the four synchrotron data sets and the program FullProf.2k.[32] No impurity was identified in the powdered sample. All site occupancies were fixed to unity and restraints were applied. For the first refined model (Exp-R1), the restraints on interatomic distances were set to B–O: 1.50(2), B–C 1.62(2), C–C: 1.54(2) Å and on angles to O-B-O 103(4), O-B-C 113(4), C-C-C 109(4)°. In the final run, 83 parameters were refined: 51 positional, and 3 isotropic displacements (one for calcium, one for BO_3 groups, and 1 for carbonyl chains), 4 lattice parameters, 16 parameters for the 4 pseudo-Voigt-profile functions, four scale parameters and 1 preferred orientation. The final agreement factors were conventional R_{wp} between 0.044 and 0.082, R_B between 0.019 and 0.058, and global $\chi^2 = 0.99$ for the four patterns of Ca-dibutylboronate used ($a = 16.4264$ (9), $b = 8.3971$ (4), $c = 9.8642$ (6) Å and $\beta = 90.458$ (3)°). Following the DFT and NMR crystallography study of the system, the structure was refined a second time (Exp-R2) by using the same methodology, but applying more restrictive restraints (interatomic distances set to B–O 1.51(1), B–C 1.62(1), C–C 1.54(1) Å and angles set to O-B-O 105.5(1.0), O-B-C 113(1), C-C-C 114(1)°), to reach a better description of the exact location of the C atoms in the lattice. The final agreement factors were very similar as for Exp-R1: conventional R_{wp} between 0.051 and 0.093, R_B between 0.024 and 0.066 and global $\chi^2 = 1.07$ for the four patterns of Ca-butylboronate used ($a = 16.4268$ (9), $b = 8.3969$ (4), $c = 9.8644$ (6) Å and $\beta = 90.462$ (3)°). CCDC-903870 contain the supplementary crystallographic data for this paper. These data can be obtained free of charge from The Cambridge Crystallographic Data Centre via www.ccdc.cam.ac.uk/data_request/cif. The corresponding Rietveld plots are shown in Figure 1, and the refined structural parameters are summarized in Table S7, Supporting Information. A general representation of the structure is shown in Figure 1, together with details of the calcium local environment.

Solid-state NMR spectroscopic experiments: ^{11}B MAS NMR spectra were recorded on Varian VNMRS 400 MHz (9.4 T) and 600 MHz (14.1 T) NMR spectrometers at frequencies of 128.38 and 192.44 MHz, respectively, by using 3.2 mm Varian T3 HXY MAS probes spinning at 20 kHz. The ground sample was physically diluted in SiO_2 prior to the NMR spectroscopic measurements (with a 1:1 $Ca[C_4H_9-B(OH)_3]_2/SiO_2$ weight ratio), to reduce preferential orientation of the platelet-shaped

crystallites in the rotor, as this was found to strongly affect the 2nd order quadrupolar lineshapes (Figure S3, Supporting Information). At both fields, the temperature was regulated such that the sample temperature in rotor was 23 °C (as calibrated by using $Pb(NO_3)_2$).[35] At 9.4 T, the single-pulse experiments were performed with a ~45° solid pulse of 1.6 µs, a recycle delay of 6 s (full relaxation), and 100 kHz spinal-64 ^1H decoupling; 560 transients were recorded. At 14.1 T, the single-pulse experiment was performed with a ~45° solid pulse of 1 µs, a recycle delay of 6 s (full relaxation), and 100 kHz spinal-64 ^1H decoupling; 72 transients were recorded. ^{11}B chemical shifts were referenced to external $NaBH_4$ at $\delta = -42.05$ ppm (used as a secondary reference).

^1H–^{13}C CPMAS NMR spectra were recorded on a Varian VNMRS 600 MHz (14.1 T) spectrometer at a ^{13}C frequency of 150.83 MHz, by using a 3.2 mm Varian T3 HXY MAS probe. Here, the as-prepared sample was directly characterized without dilution in SiO_2, because no attempt to extract ^{13}C CSA parameters was performed: the spinning sidebands are very weak in intensity when spinning at 5 kHz, and disappear completely when spinning at 10 kHz. The CPMAS spectra were recorded spinning at 10 kHz, using a contact time of 2 ms (ramped pulse), and 100 kHz spinal-64 ^1H decoupling during acquisition. It should be noted that no change in relative intensity of the ^{13}C peaks was observed for contact times (CT) of 0.5 and 5 ms. The temperature was regulated during the experiments at 23 and -55 °C (temperature in the rotor, as calibrated by using $Pb(NO_3)_2$).[35] Recycle delays of 5 and 8 s were used at -55 and 23 °C, respectively, and 100 transients were recorded in both cases. Additional spectra were also recorded at temperatures between -55 and 23 °C. ^{13}C NMR spectroscopic chemical shifts were referenced externally to adamantane (used as a secondary reference), the high frequency peak being set to $\delta = 38.5$ ppm.

The $^{13}C\{^{11}B\}$ REDOR[15] NMR spectroscopic experiment (Figure S6, Supporting Information) was carried out on a Varian VNMRS 600 MHz (14.1 T) spectrometer, by using a 3.2 mm Varian T3 HXY MAS probe spinning at 10 kHz, and sample temperatures of 23 and -55 °C. The same CP conditions as for ^1H-^{13}C CPMAS were used, with a contact time of 2 ms and recycle delays of 5 and 8 s, at -55 and 23 °C, respectively. In the $^{13}C\{^{11}B\}$ REDOR experiment, a 4.8 ms total dephasing time was applied by using rotor-synchronized π pulses on ^{11}B (8 ms π pulse—measured directly on the sample). Spinal-64 ^1H decoupling (100 kHz RF) was used during the dephasing and acquisition periods. 48 transients were recorded in both cases.

Windowed-DUMBO ^1H-MAS NMR spectroscopic experiments[18] were carried out on a Varian VNMRS 600 MHz (14.1 T) spectrometer at a frequency of 599.82 MHz. The RF field strength was 100 kHz and the duration of one DUMBO element 34.4 µs, and the observation window 0.8 µs. 16 transients were acquired, with a recycle delay of 16 s. A scaling factor was applied to the frequency axis to ensure its accurate calibration. The ^1H NMR spectroscopic chemical shifts were referenced to external adamantane at $\delta = 1.8$ ppm from tetramethylsilane (TMS), used as a secondary reference.

Natural abundance ^{43}Ca MAS NMR spectra of $Ca[C_4H_9-B(OH)_3]_2$ were recorded on Varian VNMRS 400 (9.4 T) and 600 MHz (14.1 T) spectrometers at frequencies of 26.92 and 40.37 MHz, respectively. The as-prepared sample was directly characterized without dilution in SiO_2, due to the very low sensitivity of calcium-43. At 400 MHz, a 7.5 mm Varian HX MAS probe was used, spinning at 4.5 kHz. A single-pulse experiment was carried out, by using a 2.8 µs 90° solid pulse, and a recycle delay of 0.5 s. A total of 790000 transients were acquired (which corresponds to ~4.5 days of acquisition). At 600 MHz, a 9.5 mm Varian HX MAS probe was used, spinning at 4 kHz. The DFS (double frequency sweep)[17] signal-enhancement scheme was applied for sensitivity enhancement prior to a 4 µs 90° solid pulse selective for the central transition. The DFS pulses were first optimized on ^{43}Ca-enriched $Ca[C_6H_5-B(OH)_3]_2$, with a convergence sweep from 400 to 80 kHz (duration ~6 ms; RF ~8 kHz), leading to an enhancement factor of ~2. A recycle delay of 0.5 s was used, and 180000 transients were recorded (which corresponds to ~25 h of acquisition). Chemical shifts were referenced at $\delta = 0$ ppm to a 1 mol L^{-1} aqueous solution of $CaCl_2$.[16]

DFT calculations: Geometry optimizations and calculations of IR vibrational modes: The Ca-butylboronate cell with monoclinic symmetry (Figure 1) was considered. The unit cell parameters were set to the X-ray diffraction parameters. The cell parameters and the crystal symmetry (four operators) were kept fixed during geometry optimization. This constraint has been imposed so as to ensure consistency between experimental and optimized structures. While cell parameters were kept fixed, all atoms or only some types of atoms of the unit cell were optimized (see Table 1). The Exp-R1 structure was used as a starting point for positioning protons and then performing geometry optimizations.

In this project, we decided to perform calculations with the B3LYP functional, which is well suited to the study of molecular crystals and coordination polymers. The Grimme correction was included in the calculations to take into account the weak dispersion forces, as in the systems studied here, van der Waals interactions are particularly relevant to describe intermolecular forces. B3LYP-D* calculations[20] were thus performed with the massive parallel version of the periodic ab-initio Crystal09 code.[36] This methodology has been shown to be rather accurate for systems in which both van der Waals and H-bond forces are to be accounted for.[20] The hybrid B3LYP[37] functional was used with an all-electron Gaussian basis set 6-311G(d) for all elements except for Ca in which case a TZP 6211111/331111/31 set, reoptimized for a pure cation by starting from the standard set previously published[38] was employed (explicit coefficient and exponents are given in the Supporting Information, Table S8). The five tolerances setting the accuracy of the one and bi-electron integrals were set to 8 7 7 8 25. SCF convergence was set to 10^{-7} Hartree for the energy during geometry optimization; the BROYDEN scheme with default parameters (see code manual)[36] has been used to accelerate the process. The shrinking factor for sampling in the Brillouin zone of the reciprocal space net was set to 2. As previously mentioned, geometry optimizations have been performed with different constraints; in all cases cell parameters have been kept fixed to the experimental values.

To ensure consistency in the calculation methodology, the previously published structure of the Ca-phenylboronate[3] was also relaxed by using the same methodology as in the butyl case.

For both the Ca-butylboronate and Ca-phenylboronate structures, anharmonic vibrations were then calculated for the $\nu(OH)$ modes according to previous studies,[39] assuming that the $\nu(OH)$ modes are uncoupled to others.

Table 1 summarizes the structures on which geometry optimizations and calculations of IR and NMR spectroscopic data were carried out.

Calculations of NMR parameters: The NMR parameters were calculated within Kohn–Sham DFT by using the QUANTUM-ESPRESSO code[40] in which the GIPAW method[8,9] was implemented, keeping the atomic positions equal to the values previously calculated with CRYSTAL. The PBE (Perdew, Burke, and Ernzerhof) generalized gradient approximation[41] was used and the core electrons were described by norm conserving pseudopotentials[42] in the Kleinman–Bylander[43] form. The wave functions were expanded on a plane wave basis set with a kinetic energy cut-off of 1088 eV. The integral over the first Brillouin zone was performed by using a Monkhorst-Pack $2\times2\times2$ k point grid. The isotropic chemical shift δ_{iso} is defined as $\delta_{iso}=-[\sigma-\sigma_{ref}]$ in which σ is the isotropic shielding and σ_{ref} is the isotropic shielding of the same nucleus in a reference system as previously described.[3,16b,44] Diagonalisation of the symmetrical part of the calculated chemical shielding tensor provides its principal components σ_{11}, σ_{22}, σ_{33} from which the chemical shift components δ_{11}, δ_{22}, δ_{33} can be calculated. δ_{11}, δ_{22}, and δ_{33} are defined, such as $\delta_{11}\geq\delta_{22}\geq\delta_{33}$, and $\delta_{iso}=1/3(\delta_{11}+\delta_{22}+\delta_{33})$. The CSA parameters are defined by $\Omega=\sigma_{33}-\sigma_{11}\approx\delta_{11}-\delta_{33}$ and $\kappa=3(\delta_{22}-\delta_{iso})/\Omega$. The principal components V_{xx}, V_{yy}, and V_{zz} of the electric field gradient (EFG) tensor defined as $|V_{zz}|\geq|V_{xx}|\geq|V_{yy}|$ are obtained by diagonalisation of the tensor. The quadrupolar interaction can then be characterized by the quadrupolar coupling constant C_Q and the asymmetry parameter η_Q, which are defined as: $C_Q=eQV_{zz}/h$ and $\eta_Q=(V_{yy}-V_{xx})/V_{zz}$ (e is the proton charge, h Planck's constant and Q the quadrupole moment of the considered nucleus).[45] It should be noted that all NMR spectroscopic parameters were also calculated by using the PARATEC code,[46] leading to very similar results (data not shown). For chemical shift calculations, estimated errors on calculated δ_{iso} are $\delta=0.5$ for ^1H, 1.0 for ^{13}C, 1.0 for ^{11}B, and 5.0 ppm for ^{43}Ca. These values are extracted from the standard deviations obtained when correlating experimental and calculated chemical shift values on a series of reference compounds.[16b,44,47]

[1] D. G. Hall, *Boronic Acids: Preparation and Applications in Organic Synthesis Medicine and Materials*, Wiley-VCH, Weinheim, **2011**.

[2] a) R. Nishiyabu, Y. Kubo, T. D. James, J. S. Fossey, *Chem. Commun.* **2011**, *47*, 1124–1150; b) H. M. El-Kaderi, J. R. Hunt, J. L. Mendoza-Cortes, A. P. Côté, R. E. Taylor, M. O'Keeffe, O. M. Yaghi, *Science* **2007**, *316*, 268–272; c) A. P. Côté, H. M. El-Kaderi, H. Furukawa, J. R. Hunt, O. M. Yaghi, *J. Am. Chem. Soc.* **2007**, *129*, 12914–12915; d) X. Feng, L. Liu, Y. Honsho, A. Saeki, S. Seki, S. Irle, Y. Dong, A. Nagai, D. Jiang, *Angew. Chem.* **2012**, *124*, 2672–2676; *Angew. Chem. Int. Ed.* **2012**, *51*, 2618–2622; e) B. Lukose, A. Kuc, T. Heine, *Chem. Eur. J.* **2011**, *17*, 2388–2392; f) S.-Y. Ding, W. Wang, *Chem. Soc. Rev.* **2012**, DOI: 10.1039/c2cs35072f.

[3] M. Reinholdt, J. Croissant, L. Di Carlo, D. Granier, P. Gaveau, S. Bégu, J.-M. Devoisselle, P. H. Mutin, M. E. Smith, C. Bonhomme, C. Gervais, A. van der Lee, D. Laurencin, *Inorg. Chem.* **2011**, *50*, 7802–7810.

[4] a) N. Folliet, C. Roiland, S. Bégu, A. Aubert, T. Mineva, A. Goursot, K. Selvaraj, L. Duma, F. Tielens, F. Mauri, G. Laurent, C. Bonhomme, C. Gervais, F. Babonneau, T. Azais, *J. Am. Chem. Soc.* **2011**, *133*, 16815–16827; b) Y. Xiang, J. Du, *Chem. Mater.* **2011**, *23*, 2703–2717; c) J. J. Hafner, *J. Comput. Chem.* **2008**, *29*, 2044–2078; d) A. M. Walker, B. Civalleri, B. Slater, C. Mellot-Draznieks, F. Cora, C. M. Zicovich-Wilson, G. Roman-Perez, J. M. Soler, J. D. Gale, *Angew. Chem.* **2010**, *122*, 7663–7665.

[5] a) N. Almora-Barrios, N. H. De Leeuw, *Cryst. Growth Des.* **2012**, *12*, 756–763; b) S. M. Woodley, R. Catlow, *Nat. Mater.* **2008**, *7*, 937–946; c) A. Rojas, E. Martinez-Morales, C. M. Zicovich-Wilson, M. A. Camblor, *J. Am. Chem. Soc.* **2012**, *134*, 2255–2263.

[6] a) Z. Nour, H. Petitjean, D. Berthomieu, *J. Phys. Chem. C* **2010**, *114*, 17802–17811; b) H. Guesmi, D. Berthomieu, L. Kiwi-Minsker, *Catal. Commun.* **2010**, *11*, 1026–1031; c) M. Delgado, C. C. Santini, F. Delbecq, A. Baudouin, A. De Mallmann, C. Prestipino, S. Norsic, P. Sautet, J.-M. Basset, *J. Phys. Chem. C* **2011**, *115*, 6757–6763; d) R. N. Kerber, A. Kermagoret, E. Callens, P. Florian, D. Massiot, A. Lesage, C. Coperet, F. Delbecq, X. Rozanska, P. Sautet, *J. Am. Chem. Soc.* **2012**, *134*, 6767–6775.

[7] a) C. Chizallet, G. Costentin, M. Che, F. Delbecq, P. Sautet, *J. Am. Chem. Soc.* **2007**, *129*, 6442–6452; b) F. Hoffmann, M. Guengerich, P. J. Klar, M. Froeba, *J. Phys. Chem. C* **2007**, *111*, 5648–5660; c) L. Stievano, F. Tielens, I. Lopes, N. Folliet, C. Gervais, D. Costa, J.-F.

Lambert, *Cryst. Growth Des.* **2010**, *10*, 3657–3667; d) D. Laurencin, N. Almora-Barrios, N. H. de Leeuw, C. Gervais, C. Bonhomme, F. Mauri, W. Chrzanowski, J. C. Knowles, R. J. Newport, A. Wong, Z. Gan, M. E. Smith, *Biomaterials* **2011**, *32*, 1826–1837; e) C. Martineau, F. Fayon, M. R. Suchomel, M. Allix, D. Massiot, F. Taulelle, *Inorg. Chem.* **2011**, *50*, 2644–2653.

[8] a) T. Charpentier, *Solid State Nucl. Magn. Reson.* **2011**, *40*, 1–20; b) C. Bonhomme, C. Gervais, F. Babonneau, C. Coelho, F. Pourpoint, T. Azaïs, S. E. Ashbrook, J. M. Griffin, J. R. Yates, F. Mauri, C. J. Pickard, *Chem. Rev.* **2012**, *14*, 5733–5779.

[9] C. J. Pickard, F. Mauri, *Phys. Rev. B* **2001**, *63*, 245101/1.

[10] R. K. Harris, R. E. Wasylishen, M. J. Duer, *NMR Crystallography*, Wiley-VCH, Weinheim **2009**.

[11] a) M. K. Cyrański, A. Jezierska, P. Klimentowska, J. J. Panek, A. Sporzyński, *J. Phys. Org. Chem.* **2008**, *21*, 472–482; b) M. Kurt, T. Raci Sertbakan, M. Ozduran, M. Karabacak, *J. Mol. Struct.* **2009**, *921*, 178–187; c) O. Alver, *Comptes Rendus Chim.* **2011**, *14*, 446; d) O. Alver, C. Parlak, *Vibrational Spectrosc.* **2010**, *54*, 1–9; e) S.-W. Oh, J. W. E. Weiss, P. A. Kernehan, I. Korobkov, K. E. Maly, D. L. Bryce, *Magn. Reson. Chem.* **2012**, *50*, 388–401; f) J. W. E. Weiss, D. L. Bryce, *J. Phys. Chem. A* **2010**, *114*, 5119–5131.

[12] C. Bonhomme, C. Gervais, N. Folliet, F. Pourpoint, C. Coelho Diogo, J. Lao, E. Jallot, J. Lacroix, J.-M. Nedelec, D. Iuga, J. V. Hanna, M. E. Smith, Y. Xiang, J. Du, D. Laurencin, *J. Am. Chem. Soc.* **2012**, *134*, 12611–12628.

[13] C. B. A. Lima, C. Airoldi, *Solid State Sci.* **2002**, *4*, 1321–1329.

[14] a) L. Frydman, L. J. S. Harwood, *J. Am. Chem. Soc.* **1995**, *117*, 5367–5368; b) A. Medek, J. S. Harwood, L. Frydman, *J. Am. Chem. Soc.* **1995**, *117*, 12779–12787; c) J. P. Amoureux, C. Fernandez, *Solid State Nucl. Magn. Reson.* **1998**, *10*, 211–223.

[15] T. Gullion, J. Schaefer, *J. Magn. Reson.* **1989**, *81*, 196–200.

[16] a) D. L. Bryce, *Dalton Trans.* **2010**, *39*, 8593–8602; b) C. Gervais, D. Laurencin, A. Wong, F. Pourpoint, J. Labram, B. Woodward, A. P. Howes, K. J. Pike, R. Dupree, F. Mauri, C. Bonhomme, M. E. Smith, *Chem. Phys. Lett.* **2008**, *464*, 42–48; c) D. Laurencin, M. E. Smith, *Prog. Nucl. Magn. Reson. Spectrosc.* **2012**, DOI: 10.1016/j.pnmrs.2012.05.001; d) D. Laurencin, C. Gervais, A. Wong, C. Coelho, F. Mauri, D. Massiot, M. E. Smith, C. Bonhomme, *J. Am. Chem. Soc.* **2009**, *131*, 13430–13440.

[17] D. Iuga, H. Schafer, R. Verhagen, A. P. M. Kentgens, *J. Magn. Reson.* **2000**, *147*, 192–209.

[18] a) M. Leskes, P. K. Madhu, S. Vega, *Chem. Phys. Lett.* **2007**, *447*, 370–374; b) D. Sakellariou, A. Lesage, P. Hodgkinson, L. Emsley, *Chem. Phys. Lett.* **2000**, *319*, 253–260; c) A. Lesage, D. Sakellariou, S. Hediger, B. Elena, P. Charmont, S. Steuernagel, L. Emsley, *J. Magn. Reson.* **2003**, *163*, 105–113.

[19] Neutron diffraction is not straightforward for boron-containing compounds, because the ^{10}B isotope (20% natural abundance) can capture neutrons and form α-particles and ^{7}Li.

[20] B. Civalleri, C. M. Zicovich-Wilson, L. Valenzano, P. Ugliengo, *CrystEngComm* **2008**, *10*, 405–410.

[21] T. Steiner, *Angew. Chem.* **2002**, *114*, 50–80.

[22] It is noticeable that while one H-bond is present in the CaBBu phase, two had been found previously in the CaBPh phase. This is actually consistent with the fact that the relative intensity of the broad low-frequency OH bands with respect to the higher frequency ones is bigger for CaBPh than CaBBu.

[23] Discrepancies in the relative intensities of ^{13}C NMR spectroscopic signals between experimental and simulated data are due to the fact that the CPMAS experiment is not quantitative, whereas simulations on the relaxed models were performed by considering that each C atom integrates for one. For the C_1 atoms (attached to B), a further discrepancy is noticeable, because our simulations did not take into account the additional couplings between C and B (see main text).

[24] a) E. Davies, M. J. Duer, S. E. Ashbrook, J. M. Griffin, *J. Am. Chem. Soc.* **2012**, *134*, 12508–12515; b) A. L. Webber, B. Elena, J. M. Griffin, J. R. Yates, T. N. Pham, F. Mauri, C. J. Pickard, A. M. Gil, R. Stein, A. Lesage, L. Emsley, S. P. Brown, *Phys. Chem. Chem. Phys.* **2010**, *12*, 6970–6983.

[25] K. M. King, T. M. Korter, *J. Phys. Chem. A* **2012**, *116*, 6927–6934.

[26] Other classifications of different types of H bonds would qualify those of "moderate" (see ref. 21).

[27] a) T. Emmler, S. Gieschler, H. H. Limbach, G. Buntkowsky, *J. Mol. Struct.* **2004**, *700*, 29–38; b) F. Pourpoint, C. Gervais, L. Bonhomme-Coury, T. Azais, C. Coelho, F. Mauri, B. Alonso, F. Babonneau, C. Bonhomme, *Appl. Magn. Reson.* **2007**, *32*, 435–457.

[28] When the reaction is performed at reflux instead of room temperature, a mixture of several phases is obtained, as attested by the presence of new peaks at small angles on the XRD powder patterns.

[29] A. P. Hammersley, S. O. Svensson, M. Hanfland, A. N. Fitch, D. Hausermann, *High Pressure Res.* **1996**, *14*, 235–248.

[30] S. Vogel, L. Ehm, K. Knorr, G. Braun, *Adv. X-Ray Anal.* **2002**, *45*, 31–33.

[31] A. Boultif, D. Louer, *J. Appl. Crystallogr.* **2004**, *37*, 724–731.

[32] J. Rodriguez-Carvajal, *PROGRAM FullProf.2k - version 3.20*, Laboratoire Léon Brillouin (CEA-CNRS), Saclay, **2005**; Fullprof.2k manual available at http://www.ill.eu/sites/fullprof/.

[33] R. Cerny, V. Favre-Nicolin, *Zeitschrift für Kristallographie.* **2007**, *222*, 105–113.

[34] V. Favre-Nicolin, R. Cerny, *J. Appl. Crystallogr.* **2002**, *35*, 734–743.

[35] J. Brus, *Solid State Nucl. Magn. Reson.* **2000**, *16*, 151–160.

[36] R. Dovesi, V. R. Saunders, C. Roetti, R. Orlando, C. M. Zicovich-Wilson, F. Pascale, B. Civalleri, K. Doll, N. M. Harrison, I. J. Bush, P. D. Arco, M. Llunell, *CRYSTAL09 Users Manual*, University of Turin, Turin, **2009**; see http://www.crystal.unito.it..

[37] a) C. Lee, W. Yang, R. G. Parr, *Phys. Rev. B* **1988**, *37*, 785–789; b) A. D. J. Becke, *J. Chem. Phys.* **1993**, *98*, 5648–5652.

[38] A. Schäfer, H. Horn, R. Ahlrichs, *J. Chem. Phys.* **1992**, *97*, 2571–2577.

[39] F. Pascale, S. Tosoni, C. M. Zicovich-Wilson, P. Ugliengo, R. Orlando, R. Dovesi, *Chem. Phys. Lett.* **2004**, *396*, 308–315.

[40] P. Giannozzi, S. Baroni, N. Bonini, M. Calandra, R. Car, C. Cavazzoni, D. Ceresoli, L. Chiarotti Guido, M. Cococcioni, I. Dabo, A. Dal Corso, S. de Gironcoli, S. Fabris, G. Fratesi, R. Gebauer, U. Gerstmann, C. Gougoussis, A. Kokalj, M. Lazzeri, L. Martin-Samos, N. Marzari, F. Mauri, R. Mazzarello, S. Paolini, A. Pasquarello, L. Paulatto, C. Sbraccia, S. Scandolo, G. Sclauzero, P. Seitsonen Ari, A. Smogunov, P. Umari, M. Wentzcovitch Renata, *J. Phys. Condens. Matter* **2009**, *21*, 395502.

[41] J. P. Perdew, K. Burke, M. Ernzerhof, *Phys. Rev. Lett.* **1997**, *78*, 1396.

[42] N. Troullier, J. L. Martins, *Phys. Rev. B* **1991**, *43*, 1993–2006.

[43] L. Kleinman, D. Bylander, *Phys. Rev. Lett.* **1982**, *48*, 1425–1428.

[44] C. Gervais, M. Profeta, V. Lafond, C. Bonhomme, T. Azais, H. Mutin, C. J. Pickard, F. Mauri, F. Babonneau, *Magn. Reson. Chem.* **2004**, *42*, 445–452.

[45] K. J. D. MacKenzie, M. E. Smith, *Multinuclear Solid State NMR of Inorganic Materials*, Pergamon, Amsterdam, **2002**.

[46] B. Pfrommer, D. Raczkowski, A. Canning, S. G. Louie, PARATEC (PARAllel Total Energy Code), Lawrence Berkeley National Laboratory (with contributions from F. Mauri, M. Cote, Y. Yoon, C. Pickard, P. Heynes).

[47] C. Gervais, R. Dupree, K. J. Pike, C. Bonhomme, M. Profeta, C. J. Pickard, F. Mauri, *J. Phys. Chem. A* **2005**, *109*, 6960–6969.